ELSEVIER

PII: S0951-8320(97)00015-X

Reliability Engineering and System Safety **57** (1997) 31–40

0951-8320/97/$17.00

Estimating the uncertainty of a Lagrangian photochemical air quality simulation model caused by inexact meteorological input data

G. Wotawa, A. Stohl & H. Kromp-Kolb

University of Agriculture, Forestry and Renewable Natural Resources, Institute of Meteorology and Physics, A-1180 Vienna, Austria

A deterministic Lagrangian photochemical air quality simulation model was developed at the Institute of Meteorology and Physics in Vienna. As the analysis of model uncertainty is an important part of the validation strategy, a local sensitivity and a global uncertainty analysis for model output was done. The effects of meteorological input and physical parameterisations on the model output were studied, whereas uncertainties arising from emissions and chemistry will be studied in a later stage of the model validation. As a result of the analysis, distribution density functions and vertical distributions of uncertainty in the model boxes for the chemical species ozone (O_3), nitrogen dioxide (NO_2), hydrogen peroxide (H_2O_2) and peroxiacetylnitrate (PAN) were obtained. It turned out that ozone is one of the least sensitive and uncertain species in the model. Only as far as nighttime simulations in the lowest two model boxes are concerned were the uncertainty of simulated ozone concentrations considerable. A clear weather pattern dependence of uncertainty has been detected. Highest model output variations for ozone, nitrogen dioxides and hydrogen peroxide are observed during weather situations with strong westerly winds. © 1997 Elsevier Science Limited.

1 INTRODUCTION

During the Pannonian Ozone Project (POP), a Lagrangian photochemical air quality simulation model was developed at the Institute of Meteorology and Physics in Vienna in cooperation with the Austrian Research Centre Seibersdorf. This deterministic model will be used for scenario calculations to investigate reasons for high ozone concentrations in Eastern Austria and to develop abatement strategies. Based on routine meteorological forecast data supplied by the numerical weather prediction model of the European Centre for Medium-Range Weather Forecasts (ECMWF), the POP model will also serve as a forecast tool for the authorities, which have to decide on taking actions to protect the inhabitants during episodes of high ozone concentrations. For any of these aims, a comprehensive model validation strategy is necessary. Part of this strategy will be a sensitivity and uncertainty analysis to show the validity of the model output [18].

As the model will be used for decision making and development of strategies, it is important to know that the model output should not only be treated like a set of exact numbers. Alternatively, it can be seen as a set of probability distributions. In this sense, models do not give one unique answer, but various more or less probable ones.

Probability is widely used for the quantification of uncertainty [6]. Of major concern for modellers, as well as users, is the reliability of the model. Following Scott [8], reliability means adequate understanding of sub-model interactions, validation against measurements, assessment of the effects of parameter changes and estimations of uncertainties of the model predictions.

For sensitivity and uncertainty analyses, the following components are of interest:

1. Model input data (e.g., meteorological input, emission inventory)
2. Model design parameters (e.g., simulation time, model resolution, timestep)
3. Constitutive model parameters (e.g., physical parameterisations, chemical reaction scheme)
4. Initial and boundary conditions (e.g., initial pollutant concentrations).

In this study, the analyses were confined to

meteorological input data and physical parameterisations. Uncertainties arising from emission data and the chemical scheme shall be investigated later on. Sensitivity to initial pollutant concentrations and simulation time (length of air mass trajectory) was investigated by Stohl [16].

2 MODEL DESCRIPTION

The POP model is based on 96 hours backward air mass trajectories calculated from wind fields of the numerical weather prediction model operated by the European Centre for Medium-Range Weather Forecasts (ECMWF) using the trajectory model FLEXTRA [14, 15]. The computation procedure has been described by Stohl and Wotawa [13]. For the last 12 hours of transport, local trajectories calculated from high-density surface wind observations in Eastern Austria are blended with the synoptic scale ECMWF trajectories, as pollutant concentrations highly depend on local transport patterns during the last few hours of transport [11, 22].

Meteorological data along a trajectory are taken from ECMWF analyses or short term forecasts and, whenever available, from observations. Over land surfaces, the more reliable observational data are used, if the data coverage along the trajectory is sufficient. Observation based surface and boundary layer data are computed using the OML meteorological preprocessor [7]. The meteorological data assimilation procedure used for the POP model has been described by Wotawa *et al.* [21].

The POP model consists of up to 8 vertical and up to 5 horizontal boxes. In Fig. 1, the basic model concept is shown. The model simulates emissions, chemical reactions, horizontal diffusion, vertical diffusion, dry deposition, wet deposition and synoptic scale vertical exchange. In Table 1, all modules and the needed meteorological input data are listed in detail.

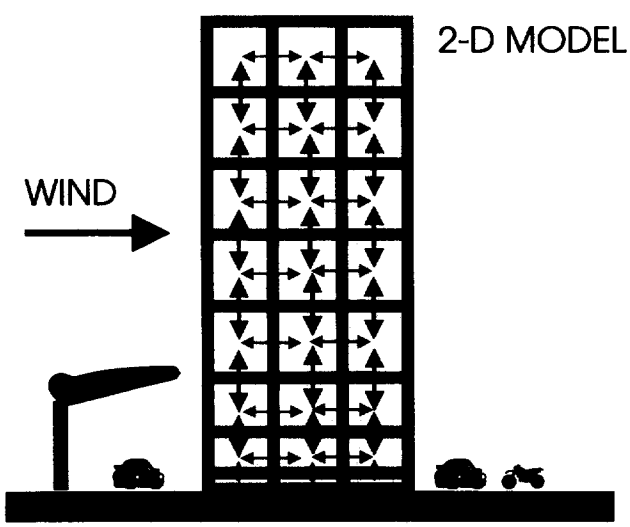

Fig. 1. Basic model concept of the POP model.

Vertical diffusion is parameterised using Monin-Obukhov theory in the surface layer and K-profile closure in the stable boundary layer and unstable outer layer [3, 17]. Horizontal diffusion is parameterised using constant exchange coefficients. Dry deposition of pollutants is simulated using surface resistances parameterised according to Wesely [19], wet deposition is parameterised using scavenging coefficients [5].

For the simulation of chemistry, three different chemical reaction mechanisms, namely CBM-IV [2], EMEP [9] and Euro-RADM [10], are available optionally. Numerical integration is done using the QSSA method [1]. European emissions are computed from the EMEP 1991 inventory (150×150 km), Austrian emissions from a recently developed high-resolution emission inventory [20] (5×5 km).

3 LOCAL SENSITIVITY ANALYSIS

Sensitivity analysis (or 'what if analysis') is defined as the computation of effects of changes in input data on the model output [4, 6]. The following meteorological input data have been included in this investigation: air temperature (*TT*), relative humidity (*RH*), boundary layer height (*Hmix*), friction velocity (*U**), surface sensible heat flux (*Fh*), precipitation rate (*RR*) and surface solar radiation (*GR*). Model output are the concentrations of the species included in the chemical scheme at the end of the 96 hour simulation period along an air mass trajectory.

For lack of computer resources, sensitivity studies were only performed using the CBM-IV mechanism, which simulates $nc = 33$ species in $nr = 88$ chemical reactions. Due to the simplifications done, CBM-IV requires less computer time than the other two chemical schemes.

Sensitivity analysis is done for a set of nt different model runs. Every model run requires one air mass trajectory with $np = 97$ trajectory positions (one position every hour of transport). $C^0_{i,j}$ are the concentrations of the model species for the nominal scenario run (= best estimate). Subscript i denotes the output species number ($i = 1,nc$), j the model run number. The best estimate model input is $X^0_{j,k,l}$. Subscript k denotes the input data number ($k = 1,nmet$), l the trajectory position number. The n-th sensitivity scenario for the m-th input means that the input is changed by a constant scenario factor $p_{m,n}$ at all trajectory positions of all model runs.

$$X^{m,n}_{j,k,l} = X^0_{j,k,l} + p_{m,n} X^0_{j,k,l} \text{ for } k = m$$

$$X^{m,n}_{j,k,l} = X^0_{j,k,l} \text{ for } k \neq m.$$

Table 1. POP model input data (trajectory position, air parcel diameter,vertical wind velocity, global radiation, 2 m air temperature, 2 m dew point, vertical temperature gradient, vertical dew point gradient, precipitation rate, surface sensible heat flux, friction velocity, boundary layer height, vegetation index) and modules (emissions, chemistry, vertical diffusion, horizontal diffusion, dry deposition, wet deposition, synoptic scale vertical exchange) for which they are used

PAR	EMIS	CHEM	VDIFF	HDIFF	DDEP	WDEP	SSVE
(X/Y/Z)	X				X		
d	X				X		
Wsyn							X
GR	X	X					
TT	X	X					
TD		X					
dT/dz		X					
dTd/dz		X					
RR						X	
HF			X	X	X		
*U**			X	X	X		
Hmix			X	X			
IVEG					X		

The sensitivity of the model output i in model run j to changes of the input m during a sensitivity scenario n is defined as follows:

$$S_{j,k,m,n} = \frac{|C^0_{i,j} - C^{m,n}_{i,j}|}{C^0_{i,j}}$$

where $S_{j,k,m,n}$ is the model output for the n-th sensitivity scenario of input m.

Afterwards, $S_{i,j,m,n}$ can be normalized by the scenario factor:

$$\tilde{S}_{i,j,m,n} = \frac{S_{i,j,m,n}}{|p_{m,n}|}.$$

The mean normalised sensitivity index $\tilde{S}_{i,m}$ of species i against input m is the average of all scenarios n of the model runs j:

$$\tilde{S}_{i,m} = MEAN(\tilde{S}_{i,j,m,n})_{j=1,nt;\ n=1,nsc}$$

where nsc is the number of sensitivity scenarios. As only the sensitivity around the nominal values is investigated, the analysis is local.

In this study, model runs were performed from 1st July 1994 0 UTC to 16th July 1994 0 UTC every 6 hours, yielding a total of $nt = 61$ runs. $nsc = 4$ sensitivity scenario runs were calculated for every model run and every input. For the estimation of uncertainty importance, the variation coefficient V_k of the input variable k was computed from available meteorological observations as an average of all trajectory positions l of all model runs j:

$$V_k = MEAN\left(\frac{\sigma_{j,k,l}}{X^0_{j,k,l}}\right)_{j=1,nt;l=1,np}.$$

The standard deviation $\sigma_{j,k,l}$ for a given trajectory position l is the empirical standard deviation of the input k from all meteorological observations, which are available within a 200 km circle around this position, whereas $X^0_{j,k,l}$ is the mean value of all observations within this circle. For all inputs k, the following sensitivity scenario factors $p_{k,n}$ were chosen:

$p_{k1} = -2V_k$
$p_{k2} = -V_k$
$p_{k3} = +V_k$
$p_{k4} = +2V_k$.

If V_k is greater than 0.4, it is set to 0.4 for the evaluation of the scenario factors.

In Table 2, mean variation coefficients V_k for all inputs k are shown. In Table 3, the mean normalised sensitivities $\tilde{S}_{i,k}$ for output species i against input k can be seen for ozone (O_3), nitrogen dioxide (NO_2), hydrogen peroxide (H_2O_2) and peroxiacetylnitrate (PAN).

Following Morgan and Henrion [6], an uncertainty importance index $U_{i,k}$ for output species i against input k is defined as the product of sensitivity and variability:

$$U_{i,k} = \tilde{S}_{i,k} V_k.$$

According to this definition, highly variable input data leading to high sensitivity of model output are most important.

In Fig. 2, the proportions of the uncertainty importances of O_3, NO_2, H_2O_2 and PAN are plotted. For NO_2, mixing height and radiation are the most important input data. As the primary pollutant NO_2 is emitted near the ground, the importance of *Hmix* indicates that NO_2 concentrations highly depend on the intensity of vertical exchange between the model layers. For O_3, H_2O_2 and PAN, friction velocity U^* is a very important input. As U^* is an essential input to the dry deposition module, the importance of this process is indicated. For O_3, radiation, temperature and mixing height are also important input data. As far as H_2O_2 is concerned, relative humidity is also

Table 2. Averaged variation coefficients V_k (%) of all meteorological input data

Input k	*TT*	*RH*	*Hmix*	*U**	*HF*	*RR*	*GR*
V_k	0.5	11.0	32.0	48.0	51.0	40.0	22.0

essential. In the case of PAN, which is thermally unstable, temperature and mixing height are the most important input data.

As can be seen, the method can give a first estimation of input data importance for crucial chemical output species of the model. In particular, the planetary boundary layer parameters *U** and *Hmix* turned out to be essential for the model, mainly due to their high variability. Unfortunately, these data are also highly uncertain [21], because their numerical values depend strongly on the used database.

Finally, an uncertainty coefficient can be calculated for every model output species i:

$$U_i = \sum_{k=1}^{nmet} U_{i,k}.$$

This coefficient can be used as a rough estimate of the total uncertainty of the model output due to the uncertainties of the input. In Fig. 3, uncertainty coefficients for O_3, NO_2, H_2O_2 and PAN are plotted. As can be seen, O_3 turned out to be the least sensitive of the four investigated output species.

4 GLOBAL UNCERTAINTY ANALYSIS

The local sensitivity analysis performed in Section 3 can only give a very rough estimate of the uncertainty of the model output species. Global uncertainty analyses have to account for the fact that the model input data can not be seen as exact numbers, but just as possible realisations of the input data space. Physical parameterisations used in the model must not be considered as exact, too. To show the consequences for model output, input data and parameterisations can be varied while a model run is repeated several times. As a result, a probability distribution of model output is obtained.

The following input data and physical parameterisations are included in the uncertainty analysis:

1. All meteorological input data investigated in Section 3
2. Trajectory position errors
3. Physical parameterisations (vertical exchange coefficients, horizontal exchange coefficients, deposition velocities and scavenging coefficients).

There are several methods of data sampling described in the relevant literature. In this study, the Monte Carlo method [4, 6] was applied. The following probability distributions of the input data and parameterisations were assumed:

1. For the meteorological input data, the empirical horizontal standard deviations Σ of all observations available within a 200 km circle around the trajectory position were calculated for all trajectory positions during the data assimilation procedure. For the Monte Carlo scenarios, the data were sampled according to the following formulation:

$$X_{i,j} = X^0_{i,j} + ndrand\sigma_{i,j}$$

where subscript i denotes the data number and j the trajectory position ($j = 1$, np). *ndrand* is a standardised normally distributed random number.

During the transport simulation along an air mass trajectory, the observations used for the calculation of model input data do not change every timestep. That means, systematic errors due to incorrect observations persist for a certain time, depending on the speed of the trajectory. To account for this, the sign of *ndrand* was left unchanged until the trajectory position was more

Table 3. Mean normalised sensitivity indices $S_{i,k}$ of model output species O_3, NO_2, H_2O_2 and PAN against changes in temperature, relative humidity, mixing height, friction velocity, surface sensible heat flux, precipitation rate and solar radiation (input parameter numbers 1–7)

SPEC	S_{i1}	S_{i2}	S_{i3}	S_{i4}	S_{i5}	S_{i6}	S_{i7}
O3	6.20	0.10	0.18	0.22	0.07	0.0043	0.22
NO2	7.90	0.16	0.50	0.14	0.13	0.0093	0.34
H2O2	25.25	0.92	0.29	0.32	0.08	0.0105	0.68
PAN	25.75	0.12	0.42	0.12	0.04	0.0065	0.28

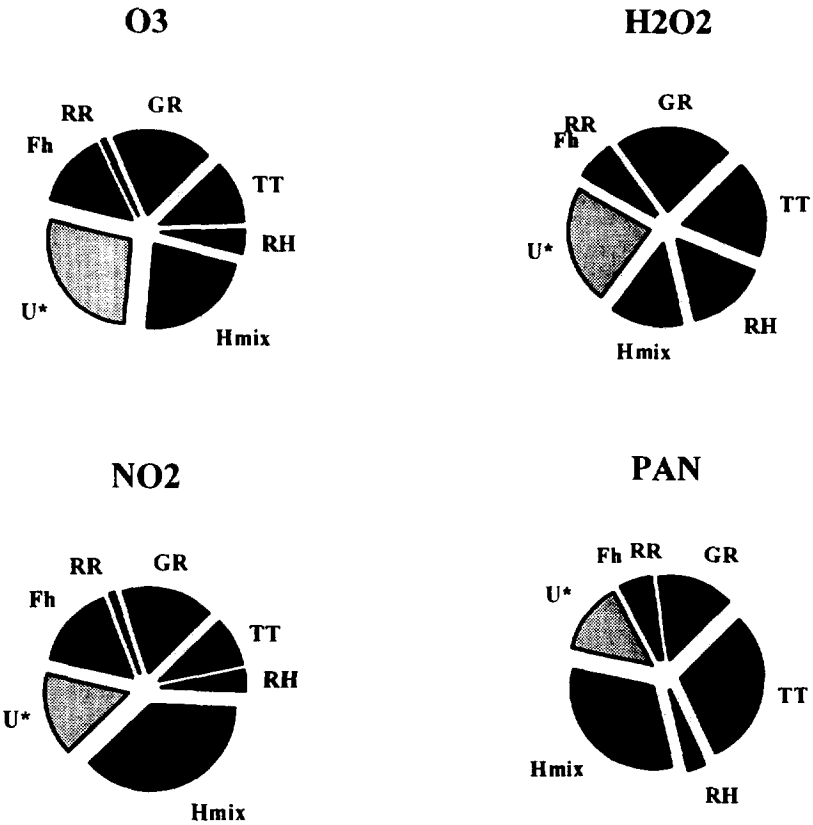

Fig. 2. Proportions of the uncertainty importance indices U_{ik} of the model output species O_3, NO_2, H_2O_2 and PAN against changes in meteorological input data.

than 100 km away from the position of last change.

2. A similar approach was carried out in the case of trajectory position errors. The nominal POP input trajectory as described by Stohl and Wotawa [13] was calculated together with two different trajectories, which account for the uncertainty of transport. Therefore, they are called uncertainty trajectories further on. The uncertainty trajectories calculated for this investigation are three dimensional trajectories starting at 200 and 800 m above ground level.

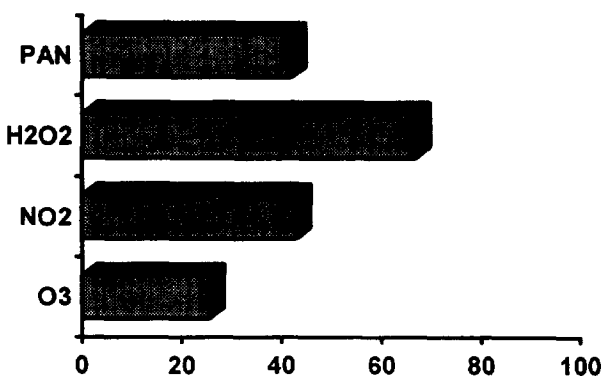

Fig. 3. Plot of uncertainty coefficients U_i (%) of the output species O_3, NO_2, H_2O_2 and PAN.

As mentioned before, the nominal trajectory and the two uncertainty trajectories were used to estimate the position error. Empirical standard deviations σ_x in longitudinal and σ_y in latitudinal direction were calculated. Afterwards, the data sampling was done using the same procedure as for the meteorological input data, with the only difference being that persistence was not assumed.

Summarising, the sampling of meteorological input data and trajectory positions accounted for the actual meteorological situation. This strategy was adopted to see whether the uncertainty depends on the weather patterns or not.

3. A somewhat different approach was used in the case of physical parameterisations. For a lack of better information, a uniform distribution between the nominal values plus and minus fixed deviations was assumed. The fixed deviations were 50% for vertical and horizontal exchange coefficients and deposition velocities and 60% for scavenging coefficients.

$$Y_i = Y_i \pm edrand\Delta Y_i$$

where Y_i is the result of the i-th parameterisation, DY_i ist the fixed deviation and *edrand* is an

equally distributed random number in the unit interval [− 1,1].

5 RESULTS OF GLOBAL UNCERTAINTY ANALYSIS

The following investigations have been carried out using the Monte Carlo version of the POP model:

1. Probability distributions of O_3, NO_2, H_2O_2 and PAN
2. Vertical distribution of uncertainty
3. Weather pattern dependence of model output uncertainty.

(i) As a result of Monte Carlo sampling, a distribution of model output species is obtained. Mean values $\overline{C_{i,j}}$ for the $k = 1$, nmc iterations of the model runs j can be calculated for every species i. For the k-th Monte Carlo iteration of model run j, the relative deviation of species i is defined as follows:

$$E_{i,j}^k = \frac{|C_{i,j}^k - \overline{C_{i,j}}|}{\overline{C_{i,j}}}.$$

Thus, distribution functions $F_i(x)$ and distribution density functions $f_i(x)$ of the relative deviations of all species $i = 1$, nc can be calculated for a single model run, or alternatively for a sample of $j = 1$, nt model runs:

$$F_i(x) = P(E_{i,j}^k \leq x) \forall_j = 1,nt;\ \forall_k = 1,nmc$$

$$f_i(x) = \frac{\partial F_i}{\partial x}.$$

Mean relative deviations $\overline{E_i}$ can also be calculated for the whole data sample.

For the calculation of $f_i(x)$, $nmc = 50$ iterations of the POP model for $nt = 41$ model runs from 1st July to 10th August 1994 12 UTC (one model run every 24 hours) were done. The same was done for 0 UTC arrival times. In Fig. 4, the distribution density function of the relative deviations for daytime (12 UTC) simulations are plotted for the species O_3, NO_2, H_2O_2 and PAN. In Fig. 5, the same is plotted for nighttime (0 UTC) simulations. From these figures, differences between daytime and nighttime simulations can be seen. As far as O_3 and H_2O_2 are concerned, the distribution functions show that larger

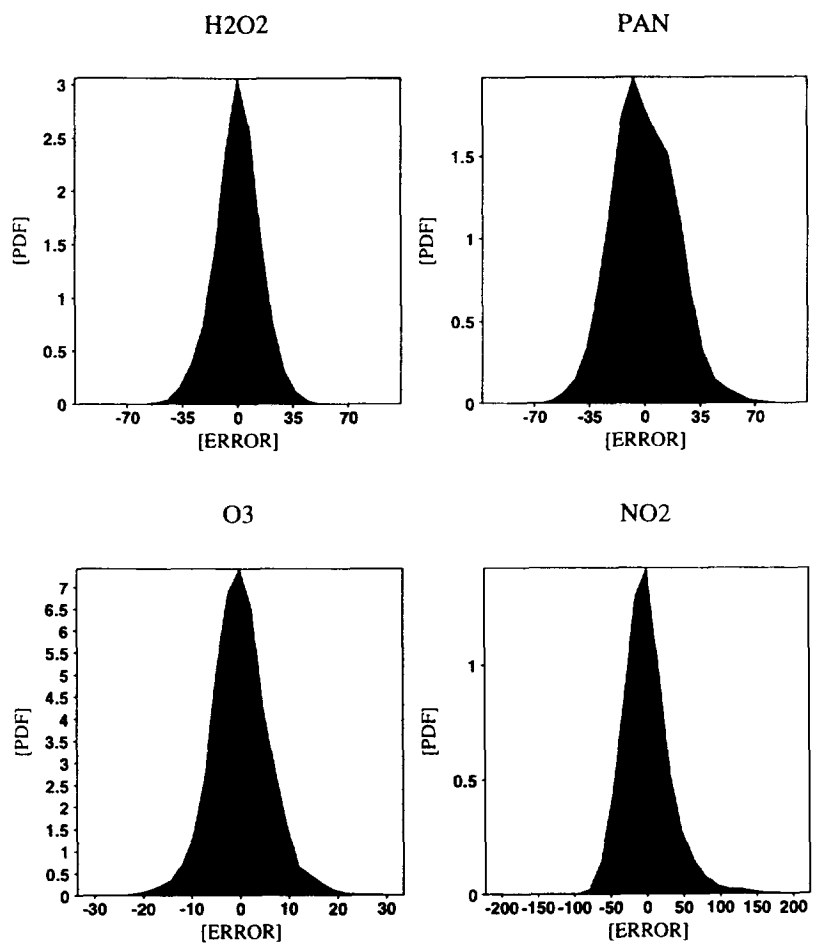

Fig. 4. Distribution density functions of relative deviations (%) for 12 UTC Monte Carlo runs for the species O_3, NO_2, H_2O_2 and PAN.

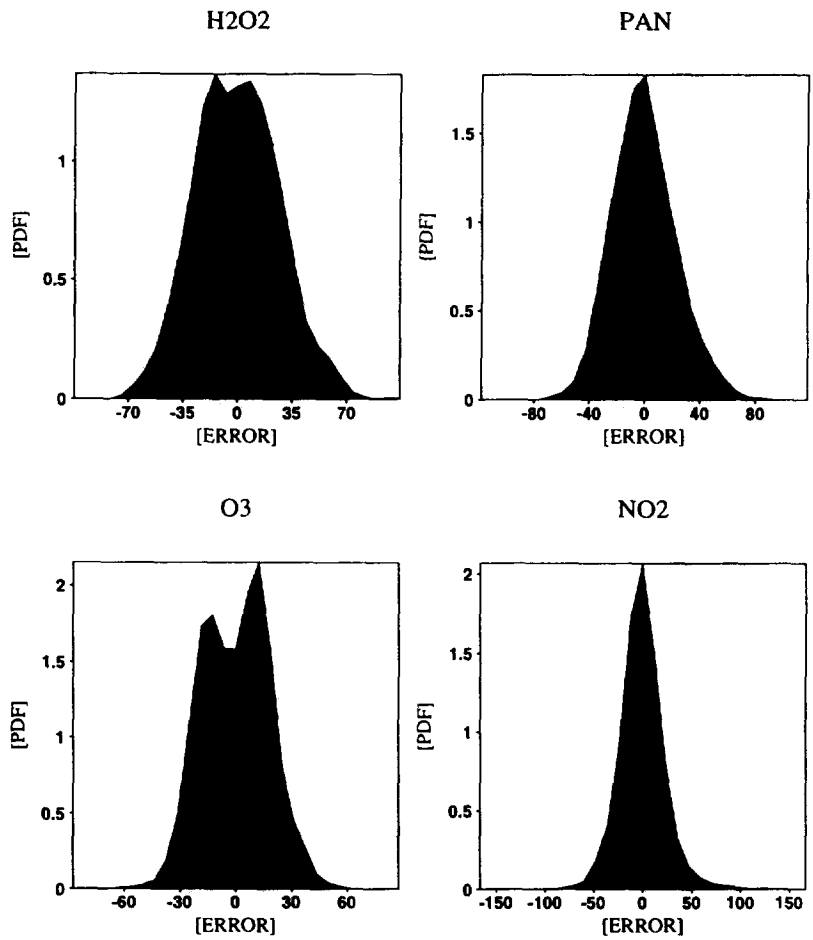

Fig. 5. Distribution density functions of relative deviations (%) for 0 UTC Monte Carlo runs for the species O_3, NO_2, H_2O_2 and PAN.

relative deviations are more frequent for nighttime than for daytime simulations. For NO_2 and PAN, the differences between day and night are substantially smaller. In Table 4, some numbers characterising the distributions are plotted, namely, mean values, 90% percentiles, 95% percentiles and 99% percentiles. In this table, the differences between 0 and 12 UTC simulations can also be seen clearly.

In Fig. 6, the vertical distribution of the mean relative deviations (model boxes 1–6) for the species O_3, NO_2, H_2O_2 and PAN is plotted for 12 UTC simulations. As far as O_3, NO_2, and H_2O_2 are concerned, the mean relative deviations decrease very slowly with the height of the model boxes. For NO_2, there is an increase, due to the fact that absolute concentrations are decreasing faster with height than the standard deviations, leading to higher relative deviations.

Table 4. Mean values, 90%, 95% and 99% percentiles characterising the distribution density functions of relative deviations (%) plotted in Figs 4 (12 UTC) and 5 (0 UTC)

	MEAN	90% PERC	95% PERC	99% PERC
O_3 12 UTC	4.5	9.4	12.4	8.1
O_3 0 UTC	15.0	27.9	33.1	45.0
NO_2 12 UTC	24.0	50.4	62.0	115.4
NO_2 0 UTC	16.7	36.5	46.2	78.9
H_2O_2 12 UTC	10.7	22.9	28.1	39.4
H_2O_2 0 UTC	21.7	42.9	52.2	65.7
PAN 12 UTC	16.1	31.6	38.3	53.7
PAN 0 UTC	18.1	37.6	45.7	62.0

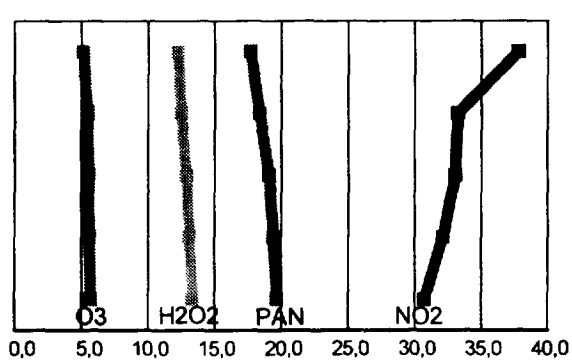

Fig. 6. Vertical distribution of mean relative deviations (%) for 12 UTC Monte Carlo runs for the species O_3, NO_2, H_2O_2 and PAN.

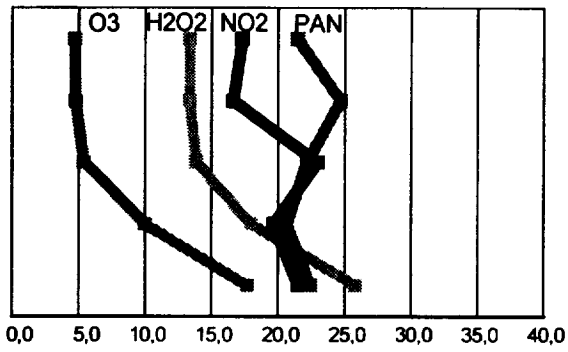

Fig. 7. Vertical distribution of mean relative deviations (%) for 0 UTC Monte Carlo runs for the species O_3, NO_2, H_2O_2 and PAN.

In Fig. 7, the same is plotted as in Fig. 6, but now for 0 UTC Monte Carlo simulations. As can be seen, there is a sharp decrease of mean relative deviations with the height of model boxes for O_3 and H_2O_2. These species show remarkably higher mean relative deviations in the lowest two model boxes for 0 UTC simulations, but the smaller values of the 12 UTC simulations are reached in model level 3.

A weather pattern classification can be done by clustering of trajectories [12]. The nominal POP trajectories for receptor point Illmitz/Burgenland from June 28th to September 30th, 1994 were used for the clustering procedure. As a distance function, the relative horizontal transport deviation [15] was used. In this investigation, four clusters were used for classification. Their respective cluster mean trajectories are plotted in Fig. 8, together with the characteristic temperature curve associated with them. Cluster I is representative for wind directions from the east, cluster II represents weak gradient weather patterns, cluster III weather patterns with higher wind speeds from the west, associated with lower temperatures. Cluster IV is representative for cases where southerly advection takes place. As only one case with southerly advection occurred from July 1st to August 10th, this cluster is excluded from the discussion. In Table 5, the mean concentrations, mean standard deviations and mean relative deviations of

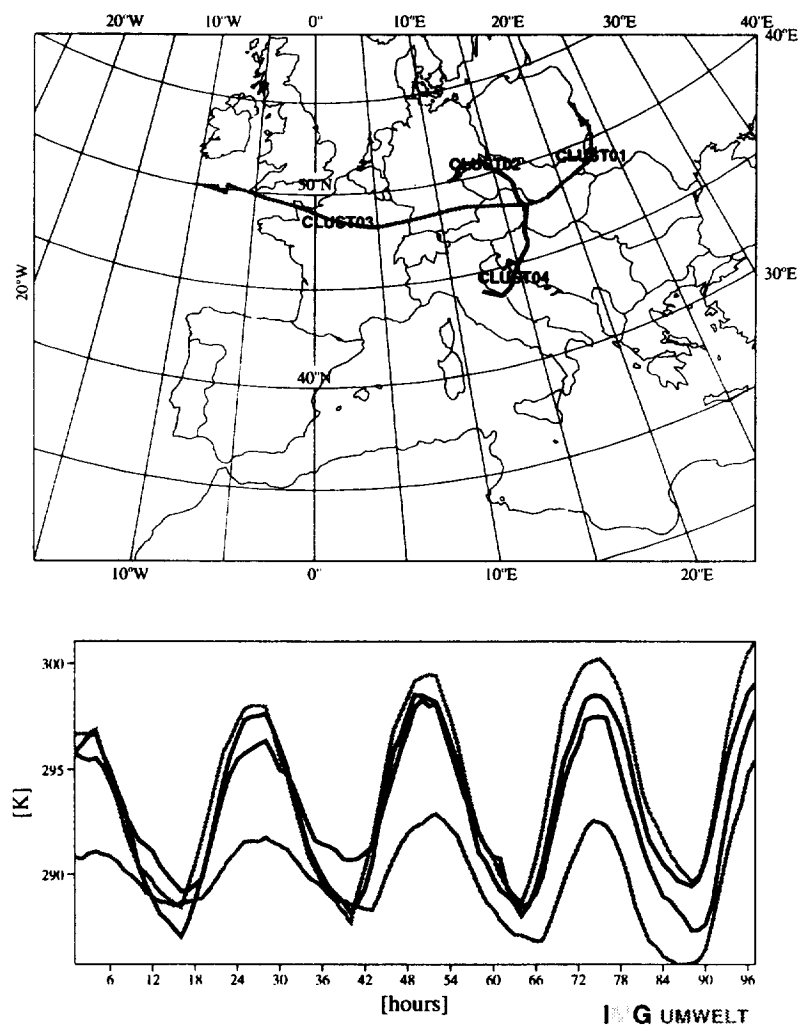

Fig. 8. Plot of cluster mean trajectories 1–4 together with the characteristic temperature development along the trajectory. These trajectories are used for weather pattern classification.

Table 5. Mean concentrations (MEAN, ppb), standard deviations (STDDEV, ppb) and mean relative deviations (RELDEV, %) of O_3, NO_2, H_2O_2 and PAN for the the weather patterns I, II and III (result of the 12 UTC Monte Carlo run)

	MEAN	STDDEV	RELDEV
		O_3	
I	60	3.0	5.0
II	68	4.0	5.9
III	57	4.6	8.3
		NO_2	
I	0.47	0.14	25.6
II	0.54	0.21	34.9
III	0.95	0.44	42.6
		H_2O_2	
I	2.8	0.32	11.8
II	3.3	0.43	13.3
III	2.0	0.36	20.7
		PAN	
I	0.7	0.13	20.9
II	1.6	0.28	18.3
III	2.1	0.38	17.1

O_3, NO_2, H_2O_2 and PAN can be seen for the weather patterns I, II and III. The table contains the results of the 12 UTC Monte Carlo run.

As can be seen, highest mean relative deviations (and therefore highest uncertainty) for all output species (except for PAN) can be found during weather pattern III, which represents cases with higher wind speeds from the west. Lowest uncertainty occurs in weather situations with moderate wind speed from eastern directions (cluster I). Weak gradient weather patterns represented by cluster II lead to somewhat higher uncertainties than analyzed in cluster I, which could be explained by higher transport deviations.

6 SUMMARY AND CONCLUSIONS

A local sensitivity analysis and a global uncertainty analysis was done for a deterministic Lagrangian air quality simulation model. Both analyses indicate that the uncertainty of model output due to inexact meteorological input data, uncertain physical parameterisations and erroneous trajectory positions is within an acceptable range. In particular, the ozone concentrations are not very sensitive to changes in input data and parameterisations. However, high uncertainty of O_3 (and H_2O_2 as well) is observed during nighttime simulations in the lowest model box. The vertical distribution obtained by the Monte Carlo runs shows that 0 UTC uncertainties of O_3 and H_2O_2 are highest in the lowest 2 model boxes, reaching almost the lower 12 UTC values in model box 3.

A clear weather pattern dependence of mean relative deviations was detected. The mean relative deviations are highest in cases where the trajectories arrive from the west. These uncertainties can be explained by:

1. higher transport deviations
2. lower boundary layer heights leading to higher primary pollutant concentrations and thus to a somewhat different chemical behaviour
3. high anthropogenic emissions from the Rhine-Ruhr Area, which are transported from the west, also leading to a different chemical behaviour.

Further uncertainty studies should include emissions, chemistry and initial pollutant concentrations to give a more complete picture of total model uncertainty. From first estimations, it can be expected that inclusion of these components in the investigation could increase the model uncertainty significantly. Some single case studies in situations with excessive model uncertainties have to be performed in order to see the reasons for this behaviour. Furthermore, the consequences of model uncertainty to forecasts, emissions reduction scenarios and design of abatement strategies have to be investigated in detail.

ACKNOWLEDGEMENT

This study has been financed by the Austrian Federal Ministries of Science, Environment and Agriculture and the governments of the Countries Vienna, Lower Austria and Burgenland as part of the Pannonian Ozone Project (POP).

REFERENCES

1. De Leeuw, F. A. A. M. and Van Rheineck Leyssius, H. J., Sensitivity of oxidant concentrations on changes in UV radiation and temperature. *Atmospheric Environment*, 1991, **25A**, 1025–1032.
2. Gery, M. W., Whitten, G. Z., Killus, J. P. and Dodge, M. C., A photochemical kinetics mechanism for urban and regional scale computer modelling. *Journal of Geophysical Research*, 1989, **94**(10), 12925–12956.
3. Holtslag, A. A. M., De Bruijn, E. I. F. and Pan, H.-L., A high resolution air mass transformation model for short-range weather forecasting. *Monthly Weather Review*, 1990, **11**(8), 1561–1575.
4. Kleijnen, J. P. C., Sensitivity analysis and related analyses: a survey of statistical techniques. Research Memorandum FEW 706, Tilburg University, The Netherlands, 1995.
5. MacMahon, T. A. and Denison, P. J., Empirical atmospheric deposition parameters—a survey. *Atmospheric Environment*, 1979, **13**, 571–585.
6. Morgan M. G. and Henrion M., *Uncertainty. A Guide to Dealing with Uncertainty in Quantitative Risk and Policy Analysis*. Cambridge University Press, Cambridge, 1990.

7. Olesen H. R. and Brown N., *The OML Meteorological Preprocessor*. National Agency of Environmental Protection, Air Pullution Laboratory, Denmark, 1988.
8. Scott E. M., Testing and assessment of environmental models. In *Proceedings of the International Symposium SAMO* 95, Beligirate, Italy, 25–27 September 1995. European Commission DGXII/D and Joint Research Centre, 1995.
9. Simpson D., Andersson-Sköld Y. and Jenkin M., Updating the chemical scheme for the EMEP MSC-W oxidant model. EMEP MSC-W Note 2/1993, Norwegian Meteorological Institute, Oslo, Norway, 1993.
10. Stockwell, W. R. and Kley, D., The Euro-RADM mechanism. A gas-phase chemical mechanism for European air quality studies. Research Center Jülich Report Jül-2868, Jülich, Germany, 1994.
11. Stohl, A. and Kromp-Kolb, H., Analyse der Ozonsituation im Grossraum Wien. *Österreichische Beiträge zu Meteorologie und Geophysik*, Heft 8, 1994.
12. Stohl, A. and Scheifinger, H., A weather pattern classification by trajectory clustering. *Meteorologische Zeitschrift N. F.*, 1994, **34,** 333–336.
13. Stohl, A. and Wotawa, G., A method for computing single trajectories representing boundary layer transport. *Atmospheric Environment*, 1995, **29,** 3235–3238.
14. Stohl A. and Wotawa G., FLEXTRA Version 1.0. Dokumentation. Institute for Meteorology and Geophysics, University of Vienna, Austria, 1994.
15. Stohl, A., Wotawa, G., Seibert, P. and Kromp-Kolb, H., Interpolation errors in wind fields as a function of spatial and temporal resolution and their impact on different types of kinematic trajectories. *Journal of Applied Meteorology*, 1995, **34,** 2149–2165.
16. Stohl A., On the use of trajectories for establishing source receptor relationships. Ph.D. thesis, University of Vienna, Austria, 1996.
17. Troen, I. B. and Mahrt, L., A simple model of the atmospheric boundary layer: sensitivity to surface evaporation. *Boundary-Layer Meteorology*, 1986, **37,** 129–148.
18. US National Research Council, *Rethinking the Ozone Problem in Urban and Regional Scale Air Pollution*. National Academy Press, Washington DC, 1989.
19. Wesely, M. L., Parameterization of surface resistances to gaseous dry deposition in regional-scale numerical models. *Atmospheric Environment*, 1989, **23A,** 1293–1304.
20. Winiwarter W. and Zueger J., Pannonisches Ozonprojekt. Teilprojekt Emissionen. Report OEFZS-A-3601, Austrian Research Center, Seibersdorf, 1995.
21. Wotawa, G., Stohl, A. and Kromp-Kolb, H., Parameterization of the planetary boundary layer over Europe—a data comparison between the observation based OML preprocessor and ECMWF model data. *Contributions to Atmospheric Physics*, 1996, **69,** 273–284.
22. Wotawa G., Stohl A. and Kromp-Kolb H., Trajektorienanalyse für Wien und Niederösterreich während einer Ozonepisode a (1992) 31.7 . Report to the Austrian Environmental Agency (Umweltbundesamt), Vienna, Austria, 1993.